ISNN:2181-1296

SHAROF RASHIDOV NOMIDAGI
SAMARQAND DAVLAT UNIVERSITETI

САМАРКАНДСКИЙ ГОСУДАРСТВЕННЫЙ
УНИВЕРСИТЕТ ИМЕНИ ШАРОФА РАШИДОВА

SAMARKAND STATE UNIVERSITY NAMED
AFTER SHAROF RASHIDOV

ILMIY AXBOROTNOMA

НАУЧНЫЙ ВЕСТНИК
SCIENTIFIC JOURNAL

ANIQ VA TABIIY FANLAR SERIYASI

Matematika, Mexanika, Informatika
Fizika, Kimyo, Biologiya, Geografiya

№ 3/2 (151)
2025

ISSN 2181-1296

ILMIY AXBOROTNOMA

НАУЧНЫЙ ВЕСТНИК SCIENTIFIC JOURNAL

2025-yil, 3-son (151/2) ANIQ VA TABIIY FANLAR SERIYASI

Matematika, Mexanika, Informatika, Fizika, Kimyo, Biologiya, Geografiya

Samarqand viloyat matbuot boshqarmasida ro‘yxatdan o‘tish tartibi 09-25.
Jurnal 1999-yildan chop qilina boshlagan va OAK ro‘yxatiga kiritilgan.

BOSH MUHARRIR **R. I. XALMURADOV, t.f.d., professor**
BOSH MUHARRIR O‘RINBOSARLARI: **H.A. XUSHVAQTOV, f-m.f.d., dotsent**

TAHRIRIYAT KENGASHI:

Sh.A.Alimov	- O‘zFA akademigi	**M.X.Ashurov**	- O‘zFA akademigi
S.N.Lakayev	- O‘zFA akademigi (SamDU)	**B.J.Axmedov**	- O‘zFA akademigi
M.M.Kamilov	- O‘zFA akademigi	**Q.G‘.G‘ulomov**	- O‘zFA akademigi
A.G.Yagola	- Moskva davlat universiteti professori (Rossiya)	**A.A.Zaxidov**	-Texas Nanotexnologiya instituti professori (AQSh)
Alberto Del Bimbo	-Florensiya universiteti professori (Italiya)	**N.B. Ferapontov**	- Moskva davlat universiteti professori (Rossiya)
Sh.Tugizov	-Kaliforniya universiteti professori (AQSh)	**V.L.Popov**	-Berlin texnika universiteti professori (Germaniya)
A.S.Soleev	- f.-m.f.d., professor (SamDU)	**N.F.Bunkin**	- Moskva davlat texnika universiteti professori (Rossiya)
I.A.Ikromov	- f.-m.f.d., professor (SamDU)	**Haji Akber Aisa**	-Xinjiang tibbiyot universiteti professori (Xitoy)
B.X.Xo‘Jayarov	- f.-m.f.d., professor (SamDU)	**E. A. Abduraxmonov**	- k.f.d., professor (SamDU)
L.Sabirov	-f.-m.f.d., professor (SamDU)	**N. K. Muxamadiyev**	- k.f.d., professor (SamDU)
A.Jumaboyev	-f.-m.f.d., professor (SamDU)	**L. A. Bulavin**	- Kiev milliy universiteti
X.Bozorov	-k.f.d., professor (SamDU)	**X. Q. Xaydarov**	- b.f.d., professor (SamDU)
O.Q.Quvondiqov	-f.-m.f.d. professor (SamDU)	**Z. I. Izzatullayev**	- b.f.d., professor (SamDU)
A.Z.Xasanov	-f.-m.f.d. professor (SamDU)	**A.B.Hasanov**	-tex.f.d., professor (SamDU)
Muhammad Suzuri bin Hitam	- Terengganu universiteti professori (Malayziya)	**Sh. T. Xoliqulov**	- q.-x.f.d., professor (SamDU)
K.D.Kuliyev	- f.-m.f .n. professor (SamDU)	**S. B. Abbosov**	- g.f.d., professor (SamDU)
A.M.Xolxo‘jayev	-f.-m.f.d., professor (SamDU)	**M.E. Mo‘minov**	-f.-m.f.d., professor (SamDU)
J.Abdullayev	-f.-m.f.d., professor (SamDU)	**I.I.Jumanov**	-tex.f.d., professor (SamDU)
A.R.Axatov	-tex.f.d., professor (SamDU)	**N.S.Mamatov**	-tex.f.d., professor (TIQXMMI)
D.B.Xursanov	- g.f.f.d., dotsent (SamDU)	**A.Sh.Yarmuxamedov**	-f-m.f.n., dotsent (SamDU)
F.Nazarov	-tex.f.f.d., dotsent (SamDU)	**X.S.Xaydarov**	-f-m.f.n., dotsent (SamDU)

Obuna indeksi – yakka tartibdagi obunachilar uchun **- 5583,**
tashkilot, korxonalar uchun **- 5584**

M U N D A R I J A
C O N T E N T S

№	Maqola nomi	Article title	Bet/ page
1	Kasr psevdoparabolik tenglama uchun Samarskiy-Ionkin ikki nuqtali chegaraviy shartlar **Sagdullaeva M.U., Xasanov G.A., Yuldashev T.K.**	Samarskii-Ionkin two-point boundary conditions for a fractional pseudoparabolic equation **Sagdullaeva M.U., Khasanov G.A., Yuldashev T.K.**	**5-14**
2	Gerasimov-Kaputo turidagi kasr tartibli nochiziqli differensial tenglamalar **Shukurova M.D., Xasanov G.A., Yuldashev T.K.**	Nonlinear differential equation with Gerasimov-Caputo type fractional operator and degenerator **Shukurova M.D., Khasanov G.A., Yuldashev T.K.**	**15-22**
3	NaH da lazer ta'sirida dissotsiatsiya dinamikasi **Umarov O., Jumabaev A.**	Laser-induced dissociation dynamics in NaH **Umarov O., Jumabaev A.**	**23-30**
4	Radon transformasidan foydalanish, tasvirni tanishda aylana sfera proyeksiyasini yaratish **Khatamov O., Mamanova B.**	Using the radon transform to create a projection of a circular sphere in image recognition **Khatamov O., Mamanova B.**	**31-38**
5	Flavonoid komplekslarining metal ionlari bilan sintezi, spektroskopik tadqiqotlar va supramolekulyar tizimlar **Ergashova Sh., Muxamadiyev N.**	Synthesis of flavonoid complexes with metal ions, spectroscopic studies and supramolecular systems **Ergashova Sh., Mukhamadiev N.**	**39-45**
6	2-benzil-6,7-dimetoksi-1,2,3,4-tetragidroizoxinolin hosilalari sintez reaksiyalarini o'rganish **Suyunova S.N., Quljonov J.X., Xudoyberdiyeva A.A., Urunbayeva Z.E. Z.E., Saidov A.Sh., Vinogradova V.I.**	Study of the reactions of synthesis of 2-benzyl-6,7-dimethoxy-1,2,3,4-tetrahydroisochinoline derivatives **Suyunova S.N., Kuljonov J.X., Khudoyberdieva A.A., Urunbaeva Z.E. Z.E., Saidov A.Sh., Vinogradova V.I.**	**46-50**
7	Keyingi qo'shni tugunlargacha o'zaro ta'sirlanuvchi ikki bozonli panjara gamiltoniani **Axmadova M., Axmatova Sh.**	A two-boson lattice hamiltonian with interactions up to next-neighboring sites **Akhmadova M., Akhmatova Sh.**	**51-58**
8	Sekin aylanishli magnitlangan neytron yulduzlarning plazma magnitosferasi o'zgartirilgan gravitatsiyada **Sayfiyev Sh.**	Plasma magnetosphere of slowly rotating magnetized neutron stars in modified gravity **Sayfiev Sh.**	**59-65**
9	Vaqtli qatorlar va mashinaviy o'qitish asosida sotuvdagi kechikishlarni aniqlash usullari **Nazarov F., Sayidqulov A.**	Methods for detecting delays in sales based on time series and machine learning **Nazarov F., Sayidkulov A.**	**66-71**
10	Integrallashgan matematik modellar va ularning qo'llanilishi **Safarov R., Xudoyberdiyev S.I.**	Integrated mathematical models and their applications **Safarov R., Khudoyberdiyev S.I.**	**72-77**
11	Chekli zichlikka va qator ko'rinishdagi moslangan manbaga ega Hirota tenglamasi uchun boshlang'ich qiymat masalasi **Eshbekov R.**	The initial value problem for the Hirota equation with finite density and self-consistent series source **Eshbekov R.**	**78-84**
12	L-sistein bilan modifikatsiyalangan mezog'ovak silikagel yordamida og'ir metall kationlarini ajratish **Ulugboyeva G.O., Kuliboyeva N.Sh., Uzokov J.R., Fazliyeva N.T., Muxamadiev N.Q.**	Removal of heavy metal cations using mesoporous silicagel modified with L-cysteine **Ulugboeva G.O., Kuliboeva N.Sh., Uzokov J.R., Fazlieva N.T., Mukhamadiev N.Q.**	**85-90**
13	Titan nano oksidi sintezi va uning fotokatalitik xossalarini zarracha o'lchamiga bog'liqligi **Mamaziyeva S., Avazova N., Tashmatova R., Muxamadiev N., Muxamadiev A., Uzokov J.**	Synthesis of nano titanium oxide and dependence of its photocatalytic properties on particle size **Mamazieva S., Avazova N., Tashmatova R., Mukhamadiev N., Mukhamadiev A., Uzokov J.**	**91-96**
14	$SrTiO_3$ nanozarrachalarini sintez qilish va ularning o'lcham-fotokatalitik xossalari **Hayitova M., Baxranova M.A., Muxamadiyev N.Q.**	Synthesis of $SrTiO_3$ and its size-dependent photocatalytic properties **Hayitova M., Bakhranova M.A., Mukhamadiyev N.Q.**	**97-102**

№	Maqola nomi	Article title	Bet/ page
15	Rekreatsiya maqsadlarida tabiatdan foydalanishni boshqarish **Rafikova N.**	Management of nature utilization for recreational purposes **Rafikova N.**	**103-110**
16	Modifikatsiyalangan faollashgan ko‘mir yordamida eritma tarkibidagi organik bo‘yoqlarni ajratish **Ergasheva D., Muxamadiyev A., Muxamadiyev N., Uzokov J.**	Separation of organic dyes from solutions using modified activated carbon **Ergasheva D., Mukhamadiyev A., Mukhamadiyev N., Uzokov J.**	**111-116**
17	Neyron tarmoqli modellar asosida qandli diabetni tashxislashning intellektual algoritmlari **Sariyev Sh.N.**	Intelligent algorithms for diagnosing diabetes mellitus based on neural network models **Sariev Sh.N.**	**117-123**
18	Mahalliy kaolindan seolitlar sintez va fizik-kimyoviy tahlili **Magdiev Sh., Majidova F., Nasimov A., Tashpulatov X., Toshpulatov D., Mirzayev Sh., Norboev K., Normuradov O.**	Synthesis and physicochemical analysis of zeolite from local kaolin **Magdiev Sh., Majidova F., Nasimov A., Tashpulatov Kh., Toshpulatov D., Mirzaev Sh., Norboev K., Normuradov O.**	**124-129**
19	Densenet modelini transfer o‘qitish asosida masofadan zondlash sahnalarini tasniflash aniqligini oshirish maqolaning o‘zbek tilidagi nomi **Yusupov O.R., Eshonqulov E.Sh.**	Enhancing the accuracy of remote sensing scene classification using transfer learning with densenet **Yusupov O.R., Eshonkulov E.Sh.**	**130-144**
20	Neft va gaz quduqlari minerallashgan qatlam suvlarining kimyoviy tarkibi va fizik-kimyoviy xususiyatlarini o‘rganish **Kenjaev N.A., Igamkulova N.A.**	Chemical composition and physico-chemical properties of mineralized formation waters from oil and gas wells **Kenjaev N.A., Igamkulova N.A.**	**145-148**

UDC: 004.93'1 **DOI:https://doi.org/10.59251/2181-3973.2025.v1.138.1.3566**

USING THE RADON TRANSFORM TO CREATE A PROJECTION OF A CIRCULAR SPHERE IN IMAGE RECOGNITION

O.Khatamov, B.Mamanova
Samarkand State University named after Sharof Rashidov, Samarkand, Uzbekistan.

O.Khatamov Samarkand State University named after Sharof Rashidov, Samarkand, Uzbekistan.

Received: 08.06.2025
Revised: 26.06.2025
Accepted: 10.07.2025
Published: 31.07.2025

Publisher: Samarkand State University named after Sharof Rashidov.

Abstract. Our article is dedicated to research image reconstruction and enhancement methods in computer tomography (CT) technology. It describes in detail the processes of restoring projections and converting images to 3D volume using Radon transformation. The possibility of using X-rays taken from different angles to obtain accurate medical images is explored, where X-rays play an important role in visualizing the internal structures of objects such as the human body. Images obtained using Radon transformation are described in the form of sinograms, and image reconstruction methods are developed through them. Sinograms are also analyzed by 1D and 2D Fourier transforms using the Fourier-slice theorem, and high-resolution image reconstruction is ensured. The article also focuses on the process of image back projection, which allows you to reconstruct the image in 3D by projecting it at different angles. It has been seen that by sending light from different angles This means that we can make changes to the image and create a 3D shape, and doing this from multiple angles will also allow us to make the image appear 3D, even when there is a shadow cast from behind.

Keywords: sinogram, computer tomography, Radon, backprojection, reconstructed image, single object, picture, shadow, trajectory.

Radon transformasidan foydalanish, tasvirni tanishda aylana sfera proyeksiyasini yaratish

Annotatsiya. Maqola kompyuter tomografiyasi (KT) texnologiyasida tasvirni qayta tiklash va yaxshilash usullarini tadqiq qilishga bag‘ishlangan. Unda proeksiyalarni tiklash va Radon transformatsiyasi yordamida tasvirlarni 3D hajmga o‘tkazish jarayonlarini batafsil tavsiflangan. Tibbiy tasvirlarni olish uchun turli burchaklardan olingan rentgen nurlaridan foydalanish imkoniyati o‘rganiladi, bu maqolada rentgen nurlari inson tanasi kabi ob'yektlarning ichki tuzilmalarini ko‘rishda muhim rol o‘ynaydi. Radon transformatsiyasi yordamida olingan tasvirlar sinogrammalar shaklida tasvirlanadi va ular orqali tasvirni qayta tiklash usullari ishlab chiqiladi. Sinogrammalar, shuningdek, Furye teoremasidan foydalangan holda 1D va 2D Furye transformatsiyalari bilan tahlil qilinadi va yuqori aniqlikdagi tasvirni qayta qurish ta'minlanadi. Maqolada, shuningdek, tasvirni turli burchaklarda proyeksiyalash orqali 3D formatida rekonstruksiya qilish imkonini beruvchi tasvirni orqaga proyeksiyalash jarayoniga e’tibor qaratilgan. Ko‘rinib turibdiki, turli burchaklardan yorug‘lik yuborish orqali bu tasvirga o‘zgartirishlar kiritilishi va 3D shakl yaratilishi mumkinligini anglatadi va buni bir necha burchakdan qilish ham orqadan soya bo‘lsa ham tasvirni 3D ko‘rinishiga olib keladi.

Kalit so‘zlar: sinogram, kompyuter tomografiyasi, Radon, orqa proyeksiya, rekonstruksiya qilingan tasvir, yagona obyekt,

rasm, soya, trayektoriya.

Использование преобразования радона для создания проекции круговой сферы при распознавании изображений

Аннотация. Статья посвящена исследованию методов реконструкции и улучшения изображений в технологии компьютерной томографии (КТ). Подробно описываются процессы восстановления проекций и преобразования изображений в 3D-объем с использованием преобразования Радона. Изучается возможность использования рентгеновских лучей, полученных под разными углами, для получения точных медицинских изображений, где рентгеновские лучи играют важную роль в визуализации внутренних структур таких объектов, как человеческое тело. Изображения, полученные с использованием преобразования Радона, описываются в виде синограмм, и на их основе разрабатываются методы реконструкции изображений. Синограммы также анализируются с помощью 1D- и 2D-преобразований Фурье с использованием теоремы о срезе Фурье, и обеспечивается реконструкция изображений с высоким разрешением. В статье также уделяется внимание процессу обратной проекции изображения backprojection, которая позволяет реконструировать изображение в 3D, проецируя его под разными углами. Было замечено, что, посылая свет под разными углами, мы можем вносить изменения в изображение и создавать трехмерную форму, а выполнение этого под разными углами также позволит нам сделать изображение трехмерным, даже если сзади отбрасывается тень.

Ключевые слова: синограмма, компьютерная томография, Радон, обратная проекция, реконструированное изображение, одиночный объект, изображение, тень, траектория.

Introduction. Nowadays, as the role of Radon transform in image restoration and noise reduction, it can be said that Radon transform is a key technology for 3D image reconstruction. This method allows to improve the quality of the image by reconstructing projections from different angles through sinograms.

Using sinograms and the Fourier-slice theorem, new algorithms are proposed for reconstructing projections using sinograms and generating accurate and efficient images through 1D and 2D Fourier transforms. This theorem makes it possible to reconstruct the image from different angles.

Significant work is being done using the backprojection method, and image restoration and resolution enhancement through backprojection techniques have been discussed. This method combines projections from different angles to form a 3D image.

The problem of increasing the clarity of files and images, while restoring the images to their original state, is relatively simple in terms of orientation, and we can explain it in simple, visual ways without resorting to mathematical formulas and equations. First, let's look at Figure 1-(a) to understand the generality of the given image. To understand the study of a single object in a general background, let's take this image as a cross-section of a human body part and its 3-dimensional shape. It is proportional to each other and at the same time can absorb high X-rays relative to itself and has such properties.

We can estimate how much of the light is absorbed by the object. Using the absorption frequency lines of X-rays emitted from the other side of the image relative to the background in the normal case, the system emits a signal, and its amplitude is directly related to the amount of absorption. In other words, the strength of the signal varies in proportion to the level of absorption, i.e. the absorption profile. It is possible to consider an arbitrary A point in an image in the form of a

wavelet in a spatially related manner. The total of the absorption measurements obtained along a single ray path that corresponds to a given point in a given image is sometimes directly related to the name of the ray. At a given point, it is possible to determine whether all the information about the area under consideration is a one-dimensional absorption signal [1].

Methods. Later, it became possible to Developing the problem of determining and simplifying mathematical formulas used for processing images of the field obtained using magnetic resonance imaging. It is also applied in many fields to other computed tomography techniques, including Utilizing various imaging methods, including photon emission tomography, positron emission tomography, magnetic resonance imaging, and ultrasound, which are all advanced techniques used to capture detailed internal images, which are currently used in mainstream medicine [2].

Before moving on to the next step, we will see how Radon transform is applied to derive an analytical formula for calculating the projection of the sphere, as illustrated in Figure 1, which appears as a circle when viewed from a specific angle:

$$f(x,y) = \begin{cases} Ax^2 + y^2 \le r^2 \\ 0otherwise \end{cases} \quad (1)$$

From this A is fixed, r is the radius of the given sphere. In this case we can consider the plane as centered with respect to the source of the circle *x,y*. Since the sphere exhibits circular symmetry, it is enough to define a unique projection for each angle relative to the projection of the sphere, which is clear from this that u = 0^0. Then equation (2) is obtained.

$$g(p,0) = \int_{-\infty}^{\infty}\int_{-\infty}^{\infty} f(x,y)\delta(x-p)dxdy = \int_{-\infty}^{\infty} f(p,y)dy \quad (2)$$

The second expression under consideration can be derived from equation (1). As mentioned in the previous expression, this expression is a line integral (hence L(p,0) with respect to the line). Additionally, it should be noted that *g(p,0)=0* when the absolute value of *p* is greater than *r*. However, when the absolute value of ppp is less than or equal to rrr, the integral is computed starting from Also, note that g(p, 0)=0 when | p|>r. When | p|≤r the integral is evaluated from $y = -(r^2 - p^2)^{1/2}$ to $y = (r^2 - p^2)^{1/2}$. Hence it is possible to obtain the plot of the Radon transformation both disc and analytically. It will also be possible to draw the transformation, since in this process, it depends on a single variable [3]. Under these conditions, g is determined by the values of *r* and *u*, the Radon function transforms into images that depend on *r* and *u*, and the variability of its points and the location of these points and the value of g that they take are determined. (Fig-1).

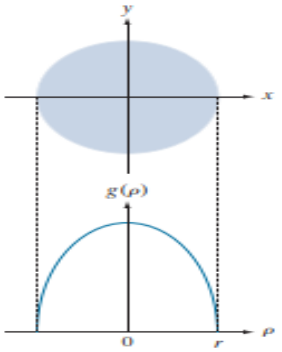


FIGURE 1. Image generation function by Radon transformation.

$$g(p,\theta) = \int_{-\sqrt{r^2-p^2}}^{\sqrt{r^2-p^2}} f(p,y)dy = \int_{-\sqrt{r^2-p^2}}^{\sqrt{r^2-p^2}} Ady \quad (3)$$

Carrying out the integration yields:

$$g(p,\theta) = g(p) = \begin{cases} 2A\sqrt{r^2-p^2} |p| \le r \\ 0otherwise \end{cases} \quad (4)$$

The transformations by the Radon function g(p,θ) are called sinograms when the images are classified into linear coordinates in the r and θ positions. The sinogram is basically represented as a Fourier spectrum and contains all the necessary information that allows us to process the original image f(x, y). The difference is that it is slightly different from the Fourier transforms, i.e., g(r,θ) is always a real function. Although sinograms are easy to interpret for simple limits, the "readability" of the problems becomes increasingly difficult as the parts of the analysis become more complex [4]. For example, the sinogram representation of the rectangle located on the left is given in Figure 2(b). In this arrangement, the vertical and horizontal axes are aligned with each other in *θ* and *r*. The bottom row

(θ=0°) represents the horizontal shadow of the rectangle, the middle row *(θ = 90°)* represents the vertical shadow. The observation that the non-zero values in the lower row are smaller compared to those in the central rows implies that the area is more constrained or narrower along the horizontal axis, or in other words, the x-axis. This suggests a reduction in width along the lateral direction.

The similarity of the linear variations of the image in both directions of view with respect to the center of the image indicates that the field is symmetrical and parallel to the x and y axes. In addition, the flatness of the sinogram means that the uniformity of the field is consistent with the variability [5]. In addition to the general work done, it is somewhat more difficult to obtain new information from a given sinogram of a new type. Figure 2 (c) shows an example of the general appearance of the Shepp-Logan phantom, which is popular for its synthetic images and the simulation of some properties and properties of the main parts of the human brain, as well as the absorption of newly formed tumors [6]. As shown in Figure 2(d), simulating the sinogram of this image poses several difficulties. Sometimes, changes due to symmetry can be inferred, but without using it, it is impossible to make higher-level inferences [7]. However, sinograms can be useful in solving problems by linking them to a learning algorithm.

Radon takes the cases that are suitable for both images and their sinograms, in addition, the lines in the sinogram are observed to correspond to angles relative to themselves on the vertical axis, while the horizontal axis, in turn, reflects values depending on the value of r. Figure 2 (c) generally depicts a Shepp-Logan phantom, which means that it exhibits a brightness that is lower than the apparent brightness. but is enlarged here for better visibility.

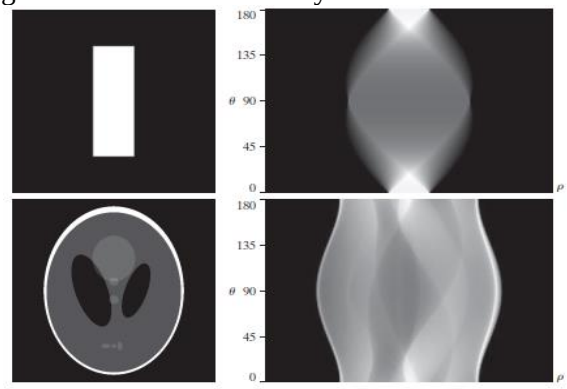


FIGURE 2. Transformation of two images and their sinogram by Radon.

To when performing the Radon transform, we generate the image backscatter by relating it to a specific expression in the image processing, in this process we define a point and start from this point, i.e., $g(p_j, \theta_k)$, from which it can be seen that the projection $g(p_j, \theta_k)$ is a sharp rotation angle from θ_k. This backscatter of this specific point involves copying the line $L(p_j, \theta_k)$into the resulting image, where the intensity of the point defined by the defined line is $g(p_j, \theta_k)$. The above process is carried out for all values of p_j projection, while keeping p_j fixed, gives the following expression:

$$f_{\theta_k}(x, y) = g(p, \theta_k) = g(xcos\theta_k + ysin\theta_k, \theta_k) \quad (5)$$

This approach forms a partial backprojected image, which can later be integrated with other projections for a complete reconstruction.

The resulting image is obtained by backprojecting the projection using the resulting angle θ_k, as shown in Figure 2(b). This formula is valid for all values of θ_k, so we have also write it more generally, the image resulting from one backprojection at the angle θ_k, the result is:

$$f_\theta(x, y) = g(xcos\theta + ysin\theta, \theta) \quad (6)$$

When we get the result, we combine all the back-projected images to produce the final image:

$$f(x, y) = \int_0^\pi f_\theta(x, y) d\theta \quad (7)$$

Becomes integral sum of the invariant states of all backprojected images:

$$f(x, y) = \sum_{\theta=0}^{\pi} f_\theta(x, y) \quad (8)$$

This is one of the fixed quantities given x, y and θ. The projections at 00 and 1800 are mirror images. The following summations are made from the initial step at 1800 to the final step. For example, the summation goes from 00 to 179.50 with an increment of 0.50. The back-projected image

thus formed is called a laminogram, which serves as an approximation of the original image obtained from the projections [8].

The following (8) was employed to create the back-projected images shown in figures 2 to 4, which were generated using this method, using the projections generated from the curves. (5). Similarly, the equations of this form were used to derive the shapes. 3(a) and (b), which correspond to sinograms of the form. 2(b) and (d). However, significant blurring is observed in the given figures, which indicates that the use of direct equations. (5) and (8) does not give satisfactory results [9]. Although the early experimental CT systems relied on these equations, substantial enhancements in the reconstruction process can be realized by rethinking and modifying the back-projection method, leading to a more efficient approach.

This section introduces the one-dimensional Fourier transform of the projection, along with the two-dimensional Fourier transform of the domain in which the projection is defined and analyzed is derived, which are integrally related to each other [10]. This work provides a basis for new construction methods that have been developed to solve previously unclear problems. Considering the one-dimensional Fourier transform of the projection with respect to the radial distance *r*, which captures the frequency components related to *r*

$$G(p,\theta) = \int_{-\infty}^{\infty} g(p,\theta) e^{-j2\pi\omega\rho} dp \quad (9)$$

in this context, ω represents frequency variable, and the equation is derived for a specific, fixed value of the angle θ, keeping it constant while evaluating the expression. By replacing with Eq.(4) into$G(p,\theta)$, the corresponding result for the given parameters is derived.

$$G(\omega,\theta) = \left[\int_{-\infty}^{\infty}\int_{-\infty}^{\infty} f(x,y) e^{-j2\pi\omega(ux+uy)}\, dxdy\right]_{u=\omega cos\theta; v=\omega sin\theta} \quad (10)$$

It seems like you're referring to the 2-D Fourier transform of a given function $f(x,y)$. The general expression for the 2-D Fourier transform of a function $f(x,y)$is given by:

$$G(\omega,\theta) = [F(u,v)]_{u=\omega cos\theta; v=\omega sin\theta} = F(\omega cos\theta, \omega sin\theta) \quad (11)$$

In this view, as always, *F(u,v)* is referred to as the 2-D Fourier transform of f(x,y).

Equation (11) is presented in the form of Fourier's theorem. As the name implies, the Fourier transform of a projection represents a component of the two-dimensional Fourier transform within the region where the projection is acquired. As illustrated in Figure 3, the connection between the projection and the one-dimensional Fourier transform is depicted, showing how the projection relates to the frequency components in that specific region.

By obtaining the values of *F(u,v)* along a line aligned with the same angle as the angle at which the projection is generated, capturing the frequency components in that specific orientation.

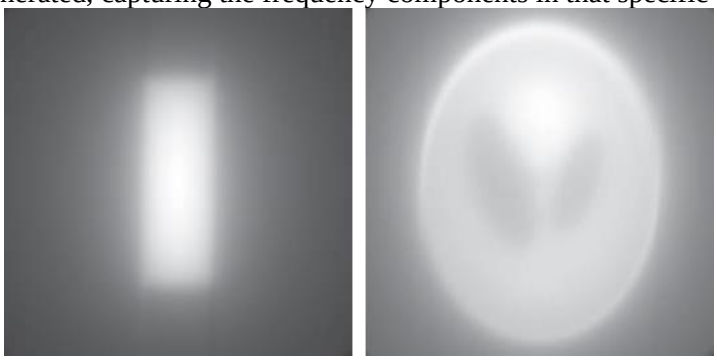


Figure 3. General view of the back-projected sinogram resulting from the random permutation.

In theory, we could retrieve *f(x,y)* by directly computing the inverse Fourier transform of *F(u,v)*. However, this process is computationally intensive, as it requires performing the inverse of a two-dimensional transform. The method described in the next section is significantly more efficient [10]. It involves organizing the use of parallel-beam filtered back projections, which reduces the computational cost and improves performance.

The expression is structured as an inverse one-dimensional Fourier transform, but it includes an additional vvv term, which serves as a one-dimensional filter transfer function. The ramp function vvv complicates the situation, as its amplitude extends infinitely in both directions, which prevents it from being integrated in a conventional manner. Since the function doesn't decay or converge to a finite value, the integration cannot be completed, leading to the inverse Fourier transform being

undefined. This makes the mathematical expression problematic and requires alternative methods to handle this issue. This is theoretically addressed using generalized delta functions [11]. Practically, the ramp is windowed to zero outside a specified frequency range, limiting the transfer function of the ramp filter.

Results. The most straightforward method to band-limit a function is by applying a box filter in the frequency domain. However, this approach introduces unwanted artifacts, such as the incoming call effects, as demonstrated in the image [12]. The first graph illustrates the ramp transfer function constrained by the box window, while the second graph shows the corresponding spatial domain representation, which is obtained by computing the inverse Fourier transform (Figure 4(a)). As anticipated, the resulting filter exhibits pronounced ringing in the spatial domain. This occurs because filtering in the frequency domain is mathematically equivalent to performing a convolution in the spatial domain. Therefore, using a function that causes ringing effects in the frequency domain inevitably results in similar ringing effects in the spatial domain. Soft function windows are used to mitigate this [13]. One example is the A discrete window function defined over *M-points*, typically used in signal processing to modify or analyze a specific portion of data, which is commonly used with a 1-D FFT to implement, and gives the following formula:

$$H(\omega) = \begin{cases} c + (c-1)cos\frac{2\pi\omega}{M} 0 \le \omega \le (M-1) \\ 0otherwise \end{cases} \quad (12)$$

When the constant ccc is set to *0.54*, the resulting function is referred to as the Hamming window. On the other hand, when ccc is equal to *0.5*, the function is known as the Hann window. These specific values of ccc define the shaping characteristics of the window functions, which are commonly used in signal processing to control the trade-off between frequency resolution and leakage. The main difference between the two is that in the Hann window, the endpoints are zero, while in the Hamming window, they are not. However, in image processing applications, this difference is usually visually imperceptible.

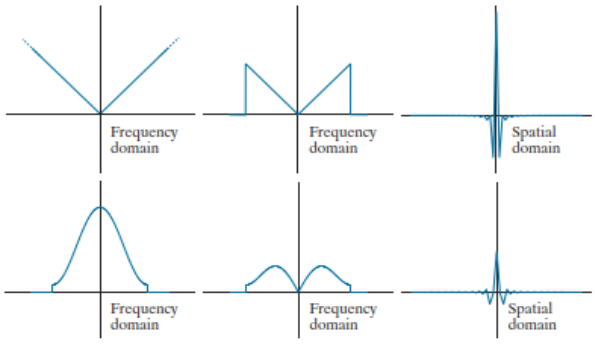


Figure 4. Frequency domain ramp filter and windowing effects.

Figure 4(d) presents a graph of the Hamming window, while Figure 4(e) illustrates the result of multiplying this window by the band-limited ramp filter transfer function shown in Figure 4(b). Figure 4(f) displays the spatial domain representation of this product, which is obtained by performing the inverse FFT (Fast Fourier Transform), as is typically done [14]. By comparing this figure with Figure 4(c), it is clear that the ringing effect has been reduced in the windowed ramp. The ratios of the peak to trough in Figures 4(c) and (f) are 2.5 and 3.4, respectively [15]. However, the central lobe in Figure 4(f) appears slightly wider than in Figure 4(c), which suggests that while backprojections using the Hamming window would result in less ringing, they might also introduce a slight blurring effect. This indicates a trade-off between reducing ringing and maintaining sharpness in the reconstruction.

As we saw in Equation (6), *G(v,u)* represents the one-dimensional Fourier transform of *g(r,u)*, which is a single projection captured at a specific angle, uuu. According to Equation (10), the full backprojected image *f(x,y)* can be obtained through the following process:

1. Calculate the one-dimensional Fourier transform for each individual projection, transforming the data from the spatial domain to the frequency domain for each projection.
2. Multiply each one-dimensional Fourier transform by the filter transfer function vvv, which, as previously described, has been scaled by an appropriate window function (such as a Hamming window) to modify its characteristics. This operation helps to shape the frequency components before proceeding with further processing.

3. Compute the inverse one-dimensional Fourier transform of each filtered transform obtained in the previous step, transforming the modified frequency-domain representation back into the spatial domain for further analysis.

4. Sum (or integrate) all of the one-dimensional inverse Fourier transforms obtained in Step 3, combining the results from each individual transform to reconstruct the complete image or signal.

The image reconstruction approach described here is known as filtered backprojection, which is commonly used in techniques like computed tomography (CT) [16]. In this method, a filter function is applied to the projection data before backprojection to improve the image quality and reduce artifacts [17].

Since data are discrete means that the information is represented by distinct, separate values or measurements, which are collected or recorded at specific intervals or points, rather than existing as a continuous flow in practice, all frequency domain operations are performed using a 1-D Fast Fourier Transform (FFT) algorithm. The filtering process is carried out in the frequency domain using the same procedure described earlier for 2-D functions [18]. This involves applying a filter to the Fourier transform of the projection data and then transforming it back to the spatial domain using the inverse FFT.

Alternatively, filtering can also be performed directly in the spatial domain using convolution. Convolution is a mathematical operation that combines the projection data with the filter function, smoothing or enhancing the data based on the characteristics of the filter. This spatial domain filtering approach is explained later in the text. Both methods aim to refine the data before backprojecting it into an image.

As with any sampled data system, important considerations must be made about the sampling rate. The selection of the sampling rate plays a crucial role in the outcomes of image processing, and it seems that there are two key factors to consider in this context. The first factor is the number of beams employed, which dictates the number of sample points in each projection. The second factor is the number of increments in the rotation angle, which influences the total number of reconstructed images. The sum of these individual images ultimately produces the final reconstructed image. Undersampling introduces bias that can appear as artefacts such as streaks in the image.

Conclusion. In general, it provides a comprehensive discussion of using the Radon transform to reconstruct projections and convert them into 3D volumes. The study focuses on how sinograms, derived from Radon transformations, can be analyzed and reconstructed into high-resolution images using Fourier transform techniques.

Key aspects covered in the article include:

- **Image reconstruction through Radon transform** to generate accurate projections from various angles.
- **Analysis of sinograms** using Fourier-slice theorem and development of high-accuracy image reconstruction methods.
- **Backprojection techniques** for creating 3D images by combining projections from different angles.
- **Noise reduction and resolution enhancement** using filters such as Hamming and Hann.

The research highlights the significance of high-quality image reconstruction for medical diagnostics, enabling detailed examination of internal structures in the human body. Additionally, the study outlines the importance of algorithms and techniques for improving CT, SPECT, and MRI technologies.

The results contribute to advancing the theoretical and practical foundations of medical imaging by offering solutions for improving diagnostic accuracy and efficiency. The article also provides recommendations for future research, emphasizing the need for continued development of more efficient image reconstruction methods.

References

1. Feng J., Cao Z, and Pi Y. “Multiphase SAR Image Segmentation With Statistical-Model-Based Active Contours,” IEEE Trans. Geoscience and Remote Sensing, vol. 51, no. 7, pp. 4190 – 4199. 2013.
2. Thurley J. M. and Danell V. “Fast Morphological Image Processing Open-Source Extensions for GPU Processing With CUDA,” IEEE J. Selected Topics in Signal Processing, 2012. vol. 6, no. 7, pp. 849–855.

3. L.-C. Chen J. T. Barron G. Papandreou, K. Murphy and A. L. Yuille, "Semantic image segmentation with task- specific edge detection using CNNs and a discriminatively trained domain transform", Proc. IEEE Conf. Comput.Vis. Pattern Recognit., pp. 4545-4554, 2016.
4. Krizhevsky A., Sutskever I., and Hinton G. E. “ImageNet Classification with Deep Convolutional Neural Networks,” Advances in Neural Information Processing Systems 25, NIPS 2012, pp. 1097–1105.
5. Beyerer J., Puente Leon F. and Frese C. Machine Vision—Automated Visual Inspection: Theory, Practice, and Applications, Springer-Verlag, Berlin, Germa New York. 2016.
6. Akhatov A., Himmatov I., Christo Ananth, Ananth Kumar. System of persons identification based on human characteristics. // Lecture Notes in Networks and Systems series. (book series) Data Management, Analytics and Innovation: Proceedings of ICDMAI 2023. Lecture Notes in Networks and Systems, 2023, 662 LNNS, pp. 1029–1046.
7. Akhatov A.R., Sabharwall M., Himmatov I.Q. Evaluation of the human pose on the basis of creating a graph of movements on the basis of a neural network. // Artificial Intelligence, Blockchain, Computing and Security - Proceedings of the International Conference on Artificial Intelligence, Blockchain, Computing and Security, ICABCS 2023, 2024, 2, pp. 668–67.
8. Fazilov S. K., Abdiyeva K. S. and Yusupov O. R. "Improvement of Image Enhancement Technique for Mammography Images," 2023 IEEE East-West Design & Test Symposium (EWDTS), Batumi, Georgia, 2023,pp. 1-5, doi: 10.1109/EWDTS59469.2023.10297044.
9. Yu H., Barriga E.S., Agurto C., Echegaray S., Pattichis M.S., Bauman W., and Soliz P. “Fast Localization and Segmentation of Optic Disk in Retinal Images Using Directional Matched Filtering and Level Sets,” IEEE Trans. Information Tech and Biomedicine,2012. vol. 16, no. 4, pp. 644 – 657.
10. Roberto Castro, Israel Pineda, Wansu Lim, and Manuel Eugenio Morocho-Cayamcela. Deep Learning Approaches Based on Transformer Architectures forImage Captioning Tasks. IEEE Access, 2022.
11. D. Liu B. Wen, Y. Fan C. C. Loy and T. S. Huang, "Non-local recurrent network for image restoration", Adv. Neural Inf. Process. Syst., pp. 1673-1682, 2018.
12. Tavboyev S., Khatamov O. " Analysis and reconstruction of noise probability density functions in images, "International Scientific and Practical Conference on Actual Problems of Mathematical Modeling and Information Technology AIP Conf. Proc. 3147, 040020-1–040020-7; https://doi.org/10.1063/5.
13. Fazilov S. K., Yusupov O.R., Abdiyeva K. S. "An Algorithm for Evaluating the Parameters Characterizing the Quality of the Image Field of the Iris by the Principal component analysis method," 2022 International Conference on Information Science and Communications Technologies (ICISCT), Tashkent, Uzbekistan, 2022,pp. 1-4, doi: 10.1109/ICISCT55600.2022.10146887.
14. Zhang Q. and Skjetne R. “Image Processing for Identification of Sea-Ice Floe Size Distribution,” IEEE Trans. Geoscience and Remote Sensing, 2015. vol. 53, no. 5, pp. 2913–2924.
15. Himmatov I., Akhatov A. Using a neural network in skeleton-based multiscale human pose estimation. // International Conference On Artificial Intellegence And Information Technologies (ICAIIT-2023) 3-4-november, Samarkand 2023.
16. Hochbaum D. “Polynomial Time Algorithms for Ratio Regions and a Variant of Normalized Cut” IEEE Trans. Pattern Anal. and Machine Intell. 2010. vol. 32, no. 5, pp. 889–898.
17. Fazilov Sh.Kh., Abdieva Kh.S., Yusupov O.R. Patch-based lesion detection using deep learning method on small mammography dataset. Artificial Intelligence, Blockchain, Computing and Security Volume 2: Proceedings of the International Conference on Artificial Intelligence, Blockchain, Computing and Security (ICABCS 2023), Gr. Noida, UP, India, 24 - 25 February 2023, pp. 643-647.
18. Liu X., Suganuma M., Sun Z., Okatani T. "Dual residual networks leveraging the potential of paired operations for image restoration", Proc. IEEE Conf. Comput. Vis. Pattern Recognit., pp. 7007-7016, 2019.